Original Article

Construction of ferroptosis and pyroptosis model to assess the prognosis of gastric cancer patients based on bioinformatics

Hanlu Shi[1#], Hongfeng Yao[2#], Yi Zhou[1#], Gaoping Wu[3], Keyi Li[1], Lusheng Tang[1], Chen Yang[1], Dong Wang[4], Weidong Jin[1]

[1]Laboratory Medicine Center, Department of Laboratory Medicine, Zhejiang Provincial People's Hospital, Affiliated People's Hospital, Hangzhou Medical College, Hangzhou, China; [2]Department of Clinical Laboratory, Zhuji People's Hospital of Zhejiang Province, Zhuji, China; [3]Department of Clinical Laboratory, Adicon Clinical Laboratories, Inc., Hangzhou, China; [4]Department of Procurement Center, Ninghai First Hospital, Ninghai, China

Contributions: (I) Conception and design: C Yang, D Wang, W Jin; (II) Administrative support: H Yao, W Jin; (III) Provision of study materials or patients: None; (IV) Collection and assembly of data: H Shi, H Yao, Y Zhou; (V) Data analysis and interpretation: G Wu, K Li, L Tang; (VI) Manuscript writing: All authors; (VII) Final approval of manuscript: All authors.

[#]These authors contributed equally to this work.

Correspondence to: Chen Yang, MD. Laboratory Medicine Center, Department of Laboratory Medicine, Zhejiang Provincial People's Hospital, Affiliated People's Hospital, Hangzhou Medical College, 158 Shangtang Road, Hangzhou 310014, China. Email: yangchendldx@163.com; Dong Wang, PhD. Department of Procurement Center, Ninghai First Hospital, 142 Taoyuan Middle Road, Ninghai 315699, China. Email: zjnhwd_8816@163.com; Weidong Jin, MD. Laboratory Medicine Center, Department of Laboratory Medicine, Zhejiang Provincial People's Hospital, Affiliated People's Hospital, Hangzhou Medical College, 158 Shangtang Road, Hangzhou 310014, China. Email: jinweidong@hmc.edu.cn.

Background: Gastric cancer (GC) is a malignancy with a grim prognosis, ranking as the second most common cause of cancer-related deaths globally. Various investigations have demonstrated the substantial involvement of ferroptosis and pyroptosis in the advancement of tumors. Nevertheless, the precise molecular mechanisms by which distinct genes associated with ferroptosis and pyroptosis influence the tumor microenvironment (TME) in GC remain elusive. Therefore, this study aims to elucidate the role of ferroptosis and pyroptosis in GC and provide insigths for GC therapy and prognosis evaluation.

Methods: The data including gene expression, clinicopathological characteristics and survival information of GC samples from The Cancer Genome Atlas (TCGA) and Gene Expression Omnibus (GEO) cohorts were collected, and the expression level of ferroptosis and pyroptosis genes (FPGs) in GC samples were analyzed. Consensus clustering analysis, Cox logistic regression, principal component analysis (PCA), and the "survival", "survminer", "limma", "ggplot2" and other packages in R were utilized to compare the differences among different groups. In the level of GC cells, cell viability experiments were conducted by Cell Counting Kit-8 (CCK-8) assay.

Results: Through the analysis of the expression level of FPGs in GC samples from the TCGA and GEO cohorts, twenty-three prognostic-related and differentially expressed FPGs were collected for further analysis. Through consensus clustering analysis, three distinct patterns of FPGs were identified and found to be correlated with clinicopathological characteristics, immune cell infiltration, and prognosis in patients with GC. Subsequently, 684 prognostic-related genes from 1,082 pattern-related differentially expressed genes (DEGs) were screened for constructing the FPG_Score system to quantify FPGs patterns in individual GC patients and predict the prognosis. The analysis indicated that GC patients with high FPG_Score exhibited improved survival rates, increased tumor mutation burden (TMB), higher microsatellite instability (MSI), and elevated programmed cell death protein ligand 1 (PD-L1) expression. These patients with high FPG_Score were more likely to benefit from immunotherapy and had a more favorable prognosis.

Conclusions: Our study innovatively provided a comprehensive analysis of FPGs in GC, and constructed the FPG_Score system for stratification of individual patients, so as to predict its benefit from immunotherapy and prognosis.

Keywords: Gastric cancer (GC); ferroptosis; pyroptosis; tumor mutational burden; microsatellite stability

Submitted Apr 24, 2024. Accepted for publication Oct 12, 2024. Published online Nov 27, 2024.
doi: 10.21037/tcr-24-683
View this article at: https://dx.doi.org/10.21037/tcr-24-683

Introduction

Gastric cancer (GC) is one of the most common malignant tumors and ranks the second leading cause of cancer-related death worldwide (1). With more than 1 million new cases estimated each year and often diagnosed at an advanced stage, GC is of a high mortality rate, with approximately 783,000 deaths reported in 2019, and the 5-year survival rate of advanced GC is less than 30% (2). Patients with early-stage GC often exhibit no symptoms, and thus missing the optimal window for elective treatment (https://www.cancer.gov/). With considerable progress in recent years in endoscopy technology, an increasing number of GC patients are being diagnosed early, but the invasiveness and expense limit large-scale GC screening. The prognosis of patients with advanced GC remains poor and poses a great burden to families and society. Therefore, there is an urgent need to better understand the molecular basis of this disease and explore effective indicators to guide diagnosis and individualized treatment strategies (3).

Programmed cell death includes apoptosis, necroptosis, ferroptosis, and pyroptosis. Induction of programmed tumor cell death plays an important role in the clinical treatment regimen of cancer. Ferroptosis is a type of programmed cell death characterized by iron-dependent lipid peroxidation, which involves the activation of reactive oxygen species (ROS), iron aggression, and degradation of cellular glutathione peroxidase 4 (GPX4) (4,5). Our previous study discovered that rat sarcoma (RAS) gene mutant tumor cells are much more sensitive to ferroptosis (6). Recently, preclinical studies have shown that ferroptosis induction has become a promising option for cancer cell death, particularly for invasive malignancies with increased levels of intracellular iron (7,8). Several ferroptosis inducers including erastin, sorafenib, and dihydroartemisinin have been screened for their ability to effectively induce ferroptosis in tumor cells (9,10). Some molecules bind directly to GPX4, promoting lipid peroxidation, and thus leading to ROS accumulation (11).

Pyroptosis is a type of programmed cell death distinct from apoptosis and is triggered by certain inflammatory vesicles, leading to gasdermin D cleavage and activation of inactive cytokines such as interleukin (IL)-18 and IL-1β (12,13). Recently, several studies have found that pyroptosis can affect tumorigenesis, cancer progression, and metastasis (14,15). Additionally, CD8 T cells kill tumor cells via pyroptosis, which may be related to the fact that pyroptosis can synergistically enhance the antitumor effects of immune checkpoint inhibitors (ICIs) (16). Deng *et al.* confirmed that histone methyltransferase inhibitor bix01294 can induce Gasdermin-E (GSDME)-mediated pyroptosis and improve the efficacy of chemotherapeutic drugs by activating autophagy in GC cells (17). Recent study has found that both ferroptosis and pyroptosis can affect the occurrence and progression of tumors. The induction of pyroptosis or ferroptosis showed synergistic antitumor activity with ICIs, even in ICI-resistant tumors (16). However, some differences exist in the characteristics of ferroptosis and pyroptosis. It has been found that anti-tumor immune cells, such as CD8 T cells, can promote these two types of cell death, simultaneously (16). CD8 T cells secret interferon-γ to induce ferroptosis, which could also promote the expression of Gasdermin-B (GSDMB) to induce pyroptosis (18,19). Liao *et al.* demonstrated that long-chain-fatty-acid-

Highlight box

Key findings

- The constructed ferroptosis and pyroptosis gene (FPG) model based on ferroptosis and pyroptosis genes will enhance the prognostic stratification of individual patients and provide a new angle for immunotherapy strategies for gastric cancer (GC) patients.

What is known and what is new?

- The importance of ferroptosis and pyroptosis in GC progression is already known.
- We first constructed the FPG model based on FPGs for predicting the prognosis and providing individualized immunotherapy for GC.

What is the implication, and what should change now?

- The gene stratification by ferroptosis and pyroptosis genes helps identify GC patients who would probably benefit from immunotherapy and predict the survival prognosis.

CoA ligase 4 (ACSL4) correlated with T-cell signatures and improved survival in immune checkpoint blockade (ICB)-treated cancer patients (20). Pyroptosis was reported to play a dual role in tumor development, either promoting tumor or causing tumor regression which depends on the context in which tumor cells are located (21). However, most studies only focused on a single ferroptosis-related gene or pyroptosis-related gene (7,14), and the comprehensive effect and tumor microenvironment (TME) infiltration characteristics mediated by the combination of ferroptosis and pyroptosis genes (FPGs) have not been fully clarified. Distinctively, we integrated ferroptosis and pyroptosis-related genes and systematically investigated the effect of two types of genes on the treatment and prognosis of GC.

In the present study, the gene expression profiles of GC patients were obtained from The Cancer Genome Atlas (TCGA) and Gene Expression Omnibus (GEO) databases. We obtained a comprehensive overview of the intratumoral immune landscape using different computational algorithms. First, GC patients were classified into three discrete patterns according to FPGs expression levels. The three patterns showed significant differences in clinical characteristics, biological processes, and immune cell infiltration. Then, patients were divided into three gene subtypes based on differentially expressed genes (DEGs) identified by three FPGs patterns. Finally, we constructed a set of scoring systems to quantify the FPGs patterns in individual patients and predict the prognosis of GC patients to ICIs treatment. Our study aims to show that FPGs play a key role in GC and would be used for predicting the prognosis and providing individualized immunotherapy for GC. We present this article in accordance with the TRIPOD reporting checklist (available at https://tcr.amegroups.com/article/view/10.21037/tcr-24-683/rc).

Methods

Data sources

A total of 806 samples (433 samples from GSE84437 and 373 samples from TCGA-GC) with complete gene expression (fragments per kilobase million, FPKM) and corresponding clinical information would be enrolled and downloaded from TCGA (available online: https://portal.gdc.cancer.gov/), (22) and GSE84437 (GEO, available online: https://www.ncbi.nlm.nih.gov/geo/) (23). We converted the FPKM values of RNA sequencing to transcripts per kilobase million (TPM) values by employing FPKM function of the "limma" package in R (24). Two datasets were combined, and batch effects were eliminated by applying the "Combat" algorithm. We drew the diagram of ferroptosis and pyroptosis copy number changes of the chromosome based on the copy number variation (CNV) using the "Rcircos" package. The study was conducted in accordance with the Declaration of Helsinki (as revised in 2013).

Consensus clustering analysis of FPGs

The FPGs were retrieved from the FerrDb (http://www.bdatjar.com:40013/bt2104/) and previous publications (25). Four hundred and thirty-four FPGs were differentially expressed between tumor and normal tissues. However, twenty-three FPGs were screened by Cox logistic regression for the significant difference in prognosis between GC tissues and their adjacent tissues and enrolled for further analysis. The "ConsensusClusterPlus" package in R was conducted for unsupervised cluster analysis to identify distinct clusters according to the expression of 23 FPGs (26).

The Human Protein Atlas (HPA)

The HPA (https://www.proteinatlas.org/) is an online database with protein immunohistochemistry information and cell-specific location of many normal and cancer tissues. We utilized it to obtain the expression level of targeted proteins in GC tissues and normal tissues according its guideline.

Identification of the relationship between clinical characteristics and FPGs patterns in GC

To investigate the clinical value of the three patterns determined by consensus clustering, we compared the relationships of clinicopathological characteristics between patterns. We evaluated the prognostic differences values of three patterns by using the Cox logistic regression model. In addition, Kaplan-Meier curves with the "survival" and "survminer" R packages were utilized to compare the prognosis among different patterns. To further explore the differences in biological processes in three patterns, gene set variation analysis (GSVA) was performed with the "GSVA" package. The gene sets of the "c2.cp.kegg.v7.4 symbol" were downloaded from the Molecular Signatures Database (MSigDB) (27). Adjusted P value <0.05 was considered statistically significant.

Estimation of TME cell infiltration of three subtypes

The single-sample gene set enrichment analysis (ssGSEA) was used to quantify the relative abundance of each immune cell infiltration in GC TME (28). The collected gene set contains various human immune cell subtypes including activated CD8 T cell, activated dendritic cell, activated B cell, macrophage, mast cells, monocyte, natural killer T cell, and regulatory T cell. The ssGSEA analysis enrichment scores were calculated to represent the relative abundance of each GC sample. The difference analysis of TME infiltrating immune cells was utilized to observe the infiltration abundance of the three subtypes.

Identification of DEGs and functional annotation

DEGs among the three FPGs patterns in GC were determined using the "limma" R package, and an adjusted P<0.05 was considered statistically significant. To identify the biological functions and related biological pathways of FPGs patterns-related DEGs, Gene Ontology (GO) and Kyoto Encyclopedia of Genes and Genomes (KEGG) pathway enrichment analysis was conducted by using the "clusterProfifiler" package in R and under the condition: false discovery rate (FDR) <0.01.

Construction of ferroptosis/pyroptosis genes signature

Principal component analysis (PCA) was used to establish the FPGs relevant risk score, termed "ferroptosis/pyroptosis score" (FPG_Score), so as to quantify the three FPGs patterns of GC patients. The procedures for the construction of FPGs signature were as follows: firstly, we used a univariate Cox logistic regression analysis to execute the prognostic analysis for all ferroptosis/pyroptosis pattern-related DEGs in the signature. Then, the "ggplot2" R package was applied to conduct PCA and construct the best FPGs prognostic signature, and the FPG_Score was calculated to quantify each GC patient. According to the median FPG_Score, GC samples were categorized into high and low groups and subjected to Kaplan-Meier survival analysis (log-rank tests, P<0.001).

Correlation between the FPG_Score and immune functions

To further clarify the relationship between FPG Score and immunity functions in GC, we applied ssGSEA to assess the abundance of tumor-infiltrating immune cells between the two FPG_Score groups and their differences in immune status. Additionally, a stratified analysis was performed to evaluate whether the FPG_Score hold its ability of prediction according to the tumor mutation burden (TMB). What's more, differential expression densities of immune checkpoints, like programmed cell death protein 1 (PD-1) and cytotoxic T lymphocyte antigen 4 (CTLA-4), between the low and high FPG_Score groups were compared using the Wilcoxon test. Furthermore, we characterized the relationships between FPG_Score and immunotherapy or microsatellite instability (MSI) by employing correlation analysis.

Cell Counting Kit-8 (CCK-8) assay

BGC823 cells were bought from Beyotime (Shanghai, China). CCK-8 assay was conducted to measure Cell viability. Briefily, Cells seeded in 96-well culture plates (Nest, Biotechnology) were administrated with different concentrations of α-ketoglutarate (α-KG) in combination with erastin at 37 ℃. After treatment, the cell supernatant was replaced with a CCK-8-containing medium for additional 2 hours. The absorbance at 450 nm was measured to reflect the viability of cells.

Statistical analysis

One-way analysis of variance (ANOVA) and the Kruskal-Wallis test were used to calculate the differences between groups. The "survminer" R package was utilized to identify the cutoff point for each dataset according to the relationship between patient survival time and FPG_Score. The difference for the survival prognosis was conducted via the Kaplan-Meier method and log-rank tests. The univariate Cox logistic regression model was employed to calculate the hazard ratios (HRs) for FPGs. PCA was used to ascertain the FPG_Score prognostic value of several clinical characteristics. For the statistical analysis of the data from *in vitro* experiment, differences were assessed with Student's *t*-test and ANOVA for comparisons between two groups and multi groups, respectively. These analyses were conducted using software of R (version 4.1.0) and GraphPad Prism (version 5.0). P<0.05 were considered statistically significant.

Results

Genetic and transcriptional alterations of differential FPGs in GC

To fully understand the gene expression patterns of FPGs in the collected 806 GC patients. A heatmap involving the expression of 202 differentially expressed FPGs between tumor and normal tissues is shown in *Figure 1A*. Among them, 23 FPGs were screened by Cox logistic regression for the significant difference in prognosis and used for subsequent analysis. Therein, HAMP, NOX3, NOX4, NOX5, and CDO1 were correlated with high hazard ratios (HRs) in patients with GC (*Figure 1B*). Then we assessed the prevalence of mutations in these 23 prognostic-related FPGs for determining the genetic alterations in mRNA levels of FPGs in GC. In the TCGA cohort, 18.24% of the GC samples harbor gene alteration in these FPGs, among them, NOX5 had the highest mutation frequency, followed by LONP1, SLC2A3, and TGFBR1 (*Figure 1C*). Next, we explored somatic copy number alterations in these FPGs and discovered prevalent copy number alterations in all 23 FPGs (*Figure 1D*). The result shows that TXNIP, MYB, CHMP4C, GLS2, AIFM2, HAMP, and ZFP36 had widespread CNV gains, while CHAC1, NNMT, CDO1, LONP1, GABARAPL1, and SLC2A3 showed CNV loss. *Figure 1E* shows the locations of the CNV alternations of the FPGs on their respective chromosomes. We further compared the expression of FPGs between GC and normal tissues. The results showed that ZFP36, DUSP1, TSC22D3, TXNIP, HBA1, GABARAPL1, and CDO1 were significantly down-regulated in tumor samples compared to those in normal samples. Additionally, results of immunohistochemistry from the HPA show most proteins were lower in GC tissues than in normal tissues (Figure S1A-S1E). However, the other 14 genes were significantly up-regulated in tumor samples, suggesting that CNV might be involved in the regulation of FPGs expression (*Figure 1F*).

FPGs patterns and clinicopathological analysis

To further explore the expression characteristics of FPGs in GC, the comprehensive landscape of FPGs interactions was visualized in a prognosis network (*Figure 2A*). We found the FPGs were correlated with each other. Then, we used a consensus clustering algorithm to categorize the patients based on the expression level of 23 FPGs. The results indicated that k=3 appeared to be an optimal selection for sorting the entire cohort into three different patterns (*Figure 2B*, Figure S2). To comprehensively master the transcriptional features of the three distinct FPGs patterns, we then conduct the PCA and observed an obvious difference in the transcription profiles of FPGs among the three clusters (*Figure 2C*). The survival analysis of the FPGs patterns showed that patients with FPGs pattern C had higher survival rates than the others (P<0.001; *Figure 2D*). In addition, comparisons among clinicopathological features and different FPGs patterns showed massive differences in FPGs expression and these features (*Figure 2E*), FPGs were high expressed in FPGs pattern A, while most genes were low expressed in FPGs pattern B.

Characteristics of TME and biological characteristics of three FPGs patterns

We performed GSVA enrichment analysis to assess the differences in biological functions of three FPGs patterns, and observed the obvious difference in functional pathways between different patterns. Indeed, FPGs pattern A was mainly concentrated in calcium signaling pathway, vascular smooth muscle contraction, and glycosphingolipid biosynthesis ganglio series; FPGs pattern B was initially associated with complement and coagulation cascades, hypertrophic cardiomyopathy, and calcium signaling pathways; FPGs pattern C was significantly associated with alanine aspartate and glutamate metabolism, base excision repair, homologous recombination, nucleotide excision repair, and DNA replication (*Figure 3A-3C*). Subsequent analysis of TME cell infiltration showed that the distribution of infiltration abundance of immune cells among three FPGs patterns was significantly discrepant (*Figure 4A*). Most of the immune cells in FPGs pattern A were higher than FPGs pattern B or C, including activated B cell, activated CD8 T cell, activated dendritic cell, eosinophil, gamma delta T cell, immature B cell, immature dendritic cell, myeloid-derived suppressor cells (MDSCs), macrophage, mast cell, natural killer T cell, natural killer cell, plasmacytoid dendritic cell, regulatory T cell, T follicular helper cell, and type 1 T helper cell, while CD56 bright natural killer cell, CD56 dim natural killer cell, monocyte, neutrophil, and type 17 T helper cell were higher infiltration in FPGs patterns B than other two FPGs patterns. These results demonstrated that the three categorized FPGs patterns harbor significantly different biological pathways and immune infiltration subtypes which could discriminate the prognosis of GC patients.

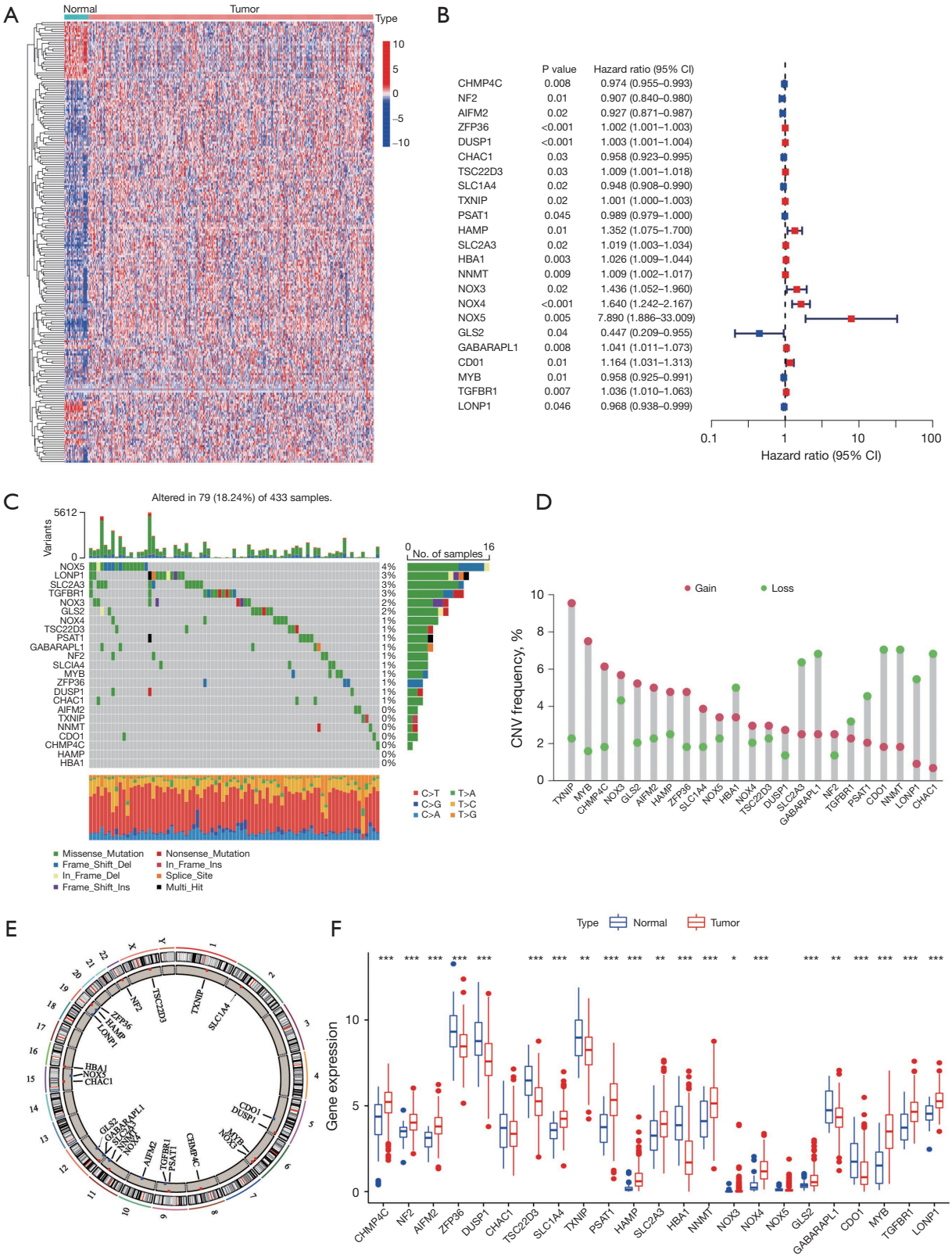

Figure 1 Genetic and transcriptional alternations of FPGs in GC. (A) Heatmap of the FPGs between the normal and the tumor tissues. Blue represents low expression level; red represents high expression level. (B) The forest plot of the univariate Cox logistic regression model

depicts the 23 statistically significant prognostic factors of FPGs in TCGA-GC cohort. Hazard ratio >1: risk factors for survival. Hazard ratio <1: protective factors for survival. (C) The mutation frequency of FPGs of GC patients in the TCGA-STAD and GSE84437 cohorts. (D) Frequencies of CNV among the FPGs. Red represents an increase in copy number, and green represents the loss of copy number. (E) Location of CNV alternations in FPGs on 23 chromosomes. (F) Expression distributions of FPGs between normal and GC tissues. ***, P<0.001; **, P<0.01; *, P<0.05. CI, confidence interval; CNV, copy number variation; FPGs, ferroptosis and pyroptosis genes; GC, gastric cancer; TCGA, The Cancer Genome Atlas; STAD, stomach adenocarcinoma.

Identification of gene subtypes based on DEGs

To further explore potential gene functions and signaling pathways among different FPGs patterns, 1,082 DEGs among the three patterns were screened employing the "limma" package (*Figure 4B*). Then, GO enrichment analysis and KEGG pathway analysis were performed based on these pattern-related DEGs. The results showed that the DEGs were mainly involved in a variety of biological functions, including nuclear division, chromosome segregation, organelle fission, and extracellular matrix organization. The cellular component in which DEGs majorly take part were the collagen-containing extracellular matrix, chromosomal region, spindle, and so on. In parallel, these DEGs were mainly involved in the molecular functions of tubulin binding, extracellular matrix structural constituent, and cytokine binding (*Figure 4C*). The KEGG enrichment analysis indicated that these DEGs major enriched in cell cycle, progesterone-mediated oocyte maturation, and DNA replication (*Figure 4D*), suggesting that subtype-related DEGs play a significant role in cell metabolism.

To further illustrate the potential biological signature of three FPGs patterns, 654 prognostic-related DEGs were screened for the consensus clustering algorithm. The GC patients were classified into three gene subtypes (gene cluster I, gene cluster II, and gene cluster III) (Figure S2). The heat map of relationships between clinicopathologic characteristics and gene subtypes revealed that the expression abundance of most prognostic-related genes was higher in gene cluster II (*Figure 4E*). Kaplan-Meier curves showed that patients with gene subtype III had the worst prognosis, whereas patients in gene cluster II showed a favorable prognosis (log-rank test, P<0.001; *Figure 4F*). As shown in *Figure 5A*, analysis of gene expression results revealed the three gene cluster subtypes showed significant differences in the expression of 23 FPGs.

Construction of the prognostic FPG_Score

To further quantify the three FPGs patterns in individual GC patients, FPG_Score was constructed based on the subtype-related gene signature in individual patients. Patients were divided into groups with low or high autophagy scores. The Sankey diagram showed the flow of the FPG_Score and illustrated the distribution of patients in the three FPGs patterns, three gene subtypes, and two FPG_Score groups (*Figure 5B*). To assess the effect of the FPG_Score on TME, we compared the infiltration of immune cells between the two FPG_Score groups. The results show that the FPG_Score was significantly positively correlated with activated CD4 T cells, neutrophils, CD56 dim natural killer cells, type 17 T helper cells, and type 2 T helper cells (*Figure 5C*). To further evaluate the clinical relevance of the FPG_Score, we performed survival analysis. Patients with high FPG_Score display a prominent survival benefit (log-rank test, P<0.001; *Figure 5D*). Moreover, the FPG_Score differed not only in the FPGs patterns but also in the gene subtypes. The FPGs pattern C and gene subtype II harbor a higher score (*Figure 5E,5F*). These results indicated that FPG_Score could be used for prognostic prediction for GC patients.

Characteristics of FPGs subtypes in TMB and immune functions

A wealth of novel research has demonstrated that ICIs have become the trend in tumor therapy (29,30). Identifying distinct TME phenotypes would be of significance to predict the response to immunotherapy. It has been shown that TMB was a predictive biomarker, which could identify cancer patients who are most likely to benefit from ICIs (31,32). To further expand the insight of FPG_Score, the application of FPG_Score in the prediction of TMB and tumor immunology therapy was investigated. Spearman correlation analysis demonstrated that the FPG_Score was positively correlated with the TMB (P<0.001; *Figure 6A*). Increasing evidence showed that higher TMB means higher numbers of neoantigens, which could predict the benefit from immunotherapy. The analysis of the mutation data in the TCGA cohort showed a higher TMB in the high FPG_

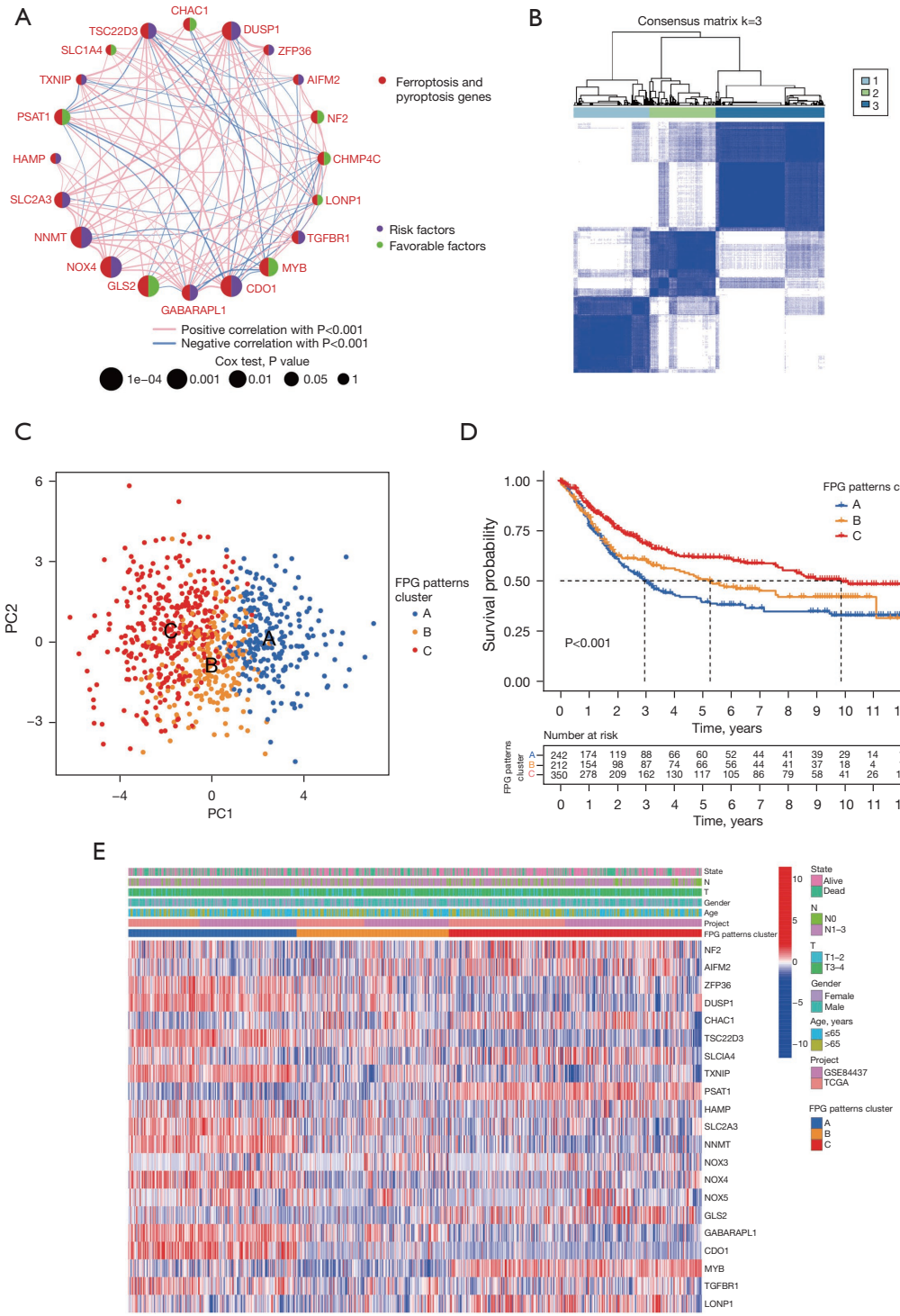

Figure 2 FPGs and clinicopathological characteristics of two distinct patterns of samples divided by consistent clustering. (A) Interactions among FPGs in GC. The line connecting the FPGs represents their interaction, and the line thickness indicates the strength of the association between FPGs. (B) The optimal number of clusters (K=3) was determined from CDF curves. (C) The scatter plot of PCA from three FPG patterns clusters. (D) Survival analysis based on the three FPGs patterns. (E) Differences in clinicopathologic features and expression levels of FPGs between three distinct patterns. FPG, ferroptosis and pyroptosis gene; TCGA, The Cancer Genome Atlas; GC, gastric cancer; PCA, principal component analysis; CDF, cumulative distribution function.

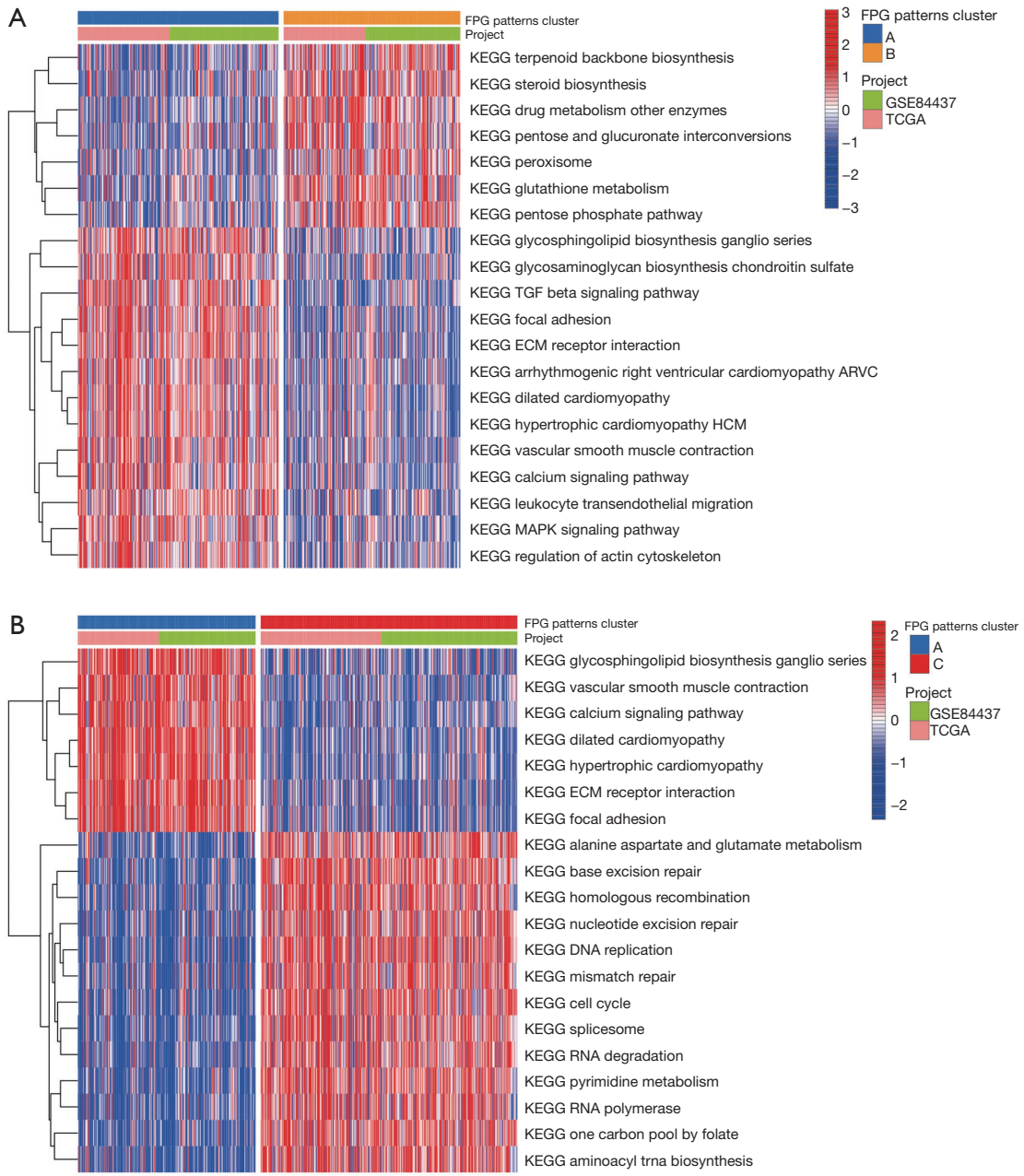

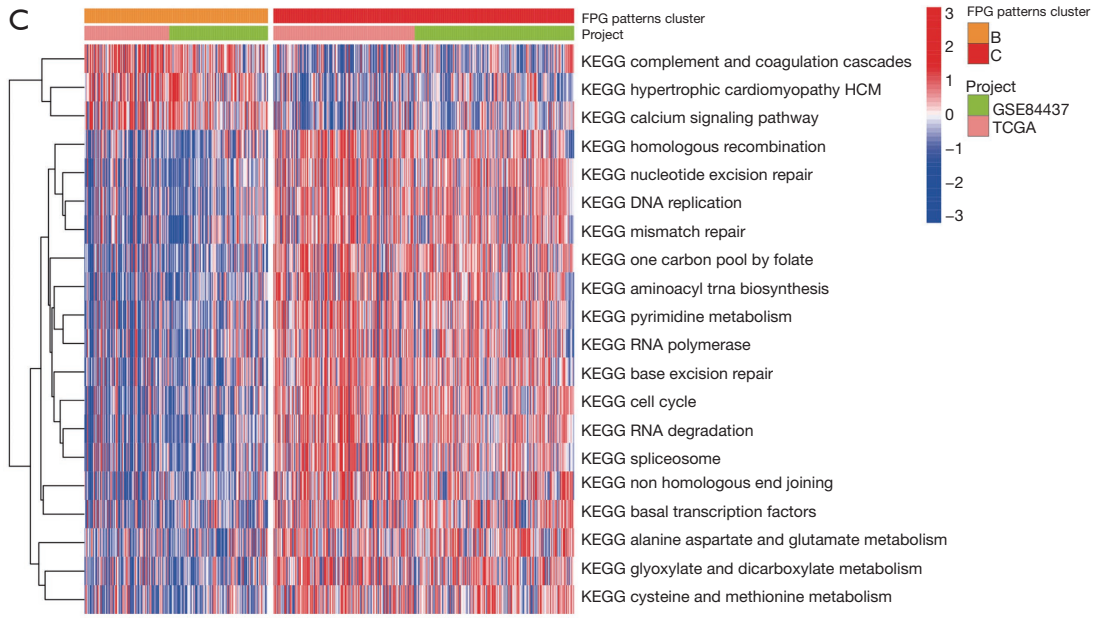

Figure 3 The biological characteristics of three FPGs patterns. (A) GSVA analyzed the differences between functional pathways in FPGs pattern A and B. (B) GSVA analyzed the differences between functional pathways in FPGs pattern A and C. (C) GSVA analyzed the differences between functional pathways in FPGs pattern B and C. Blue represents the FPGs pattern A, orange represents the FPGs pattern B and red represents the FPGs pattern C. FPG, ferroptosis and pyroptosis gene; TCGA, The Cancer Genome Atlas; KEGG, Kyoto Encyclopedia of Genes and Genomes; GSVA, gene set variation analysis.

Score group than that in low FPG_Score group (*Figure 6B*), indicating that the patients in high FPG_Score group might get benefits from immunotherapy. Subsequently, the distribution variations of the somatic mutations were analyzed between two FPG_Score groups in the TCGA cohort. The mutation frequency of the high FPG_Score group is 98.06%, which is higher than the low FPG_Score group (84.17%). The top ten mutation genes in the high and low FPG_Score groups were *TTN*, *TP53*, *MUC16*, *ARID1A*, *LRP1B*, *SYNE1*, *FLG*, *FAT4*, *CSMD3*, and *PCLO* (*Figure 6C*,*6D*). Then, GC samples were divided into high and low TMB groups according to the optimal cutoff value of TMB by using the minimum P value method. Survival analysis of TMB revealed that the prognosis of the high TMB group was better than that of patients in the low TMB group (*Figure 6E*). Moreover, the survival curves of combined TMB with the FPG_Score showed that the patients in both the high tumor mutation group and the high FPG_Score group had the best prognosis (*Figure 6F*).

Immunotherapy and MSI analysis

In recent years, with the application of targeted drugs and immunotherapeutics, such as programmed cell death protein 1/programmed cell death protein ligand 1 (PD-1/PD-L1) antibodies, the treatment efficacy of the advanced GC has increased. In addition, research has proven that the expression of PD-1 and PD-L1 is related to the therapeutic response to ICIs in GC (33). Similarly, our results manifested that the expression of PD-L1 was increased in the high FPG_Score group, while the expression of PD-1 did not differ between the high and low FPG_Score groups (*Figure 7A*,*7B*). These results suggested GC patients in the high FPG_Score group might be more sensitive to immunotherapy and thus benefit from immunotherapy drugs. Moreover, correlation analysis was performed to evaluate the effect of the FPG_Score on the survival status of GC patients, and the bar graph revealed that patients with high FPG_Score occupied a larger proportion of alive status (68%) than dead status (*Figure 7C*). Similarly, the box plots demonstrated that the FPG_Score of patients with alive status was statistically higher than that with dead status (*Figure 7D*). Kaplan-Meier analysis of survival rate showed that patients with the high FPG_Score had a better prognosis than patients with the low FPG_Score group both in the comparison of T1–T2 and T3–T4 stages

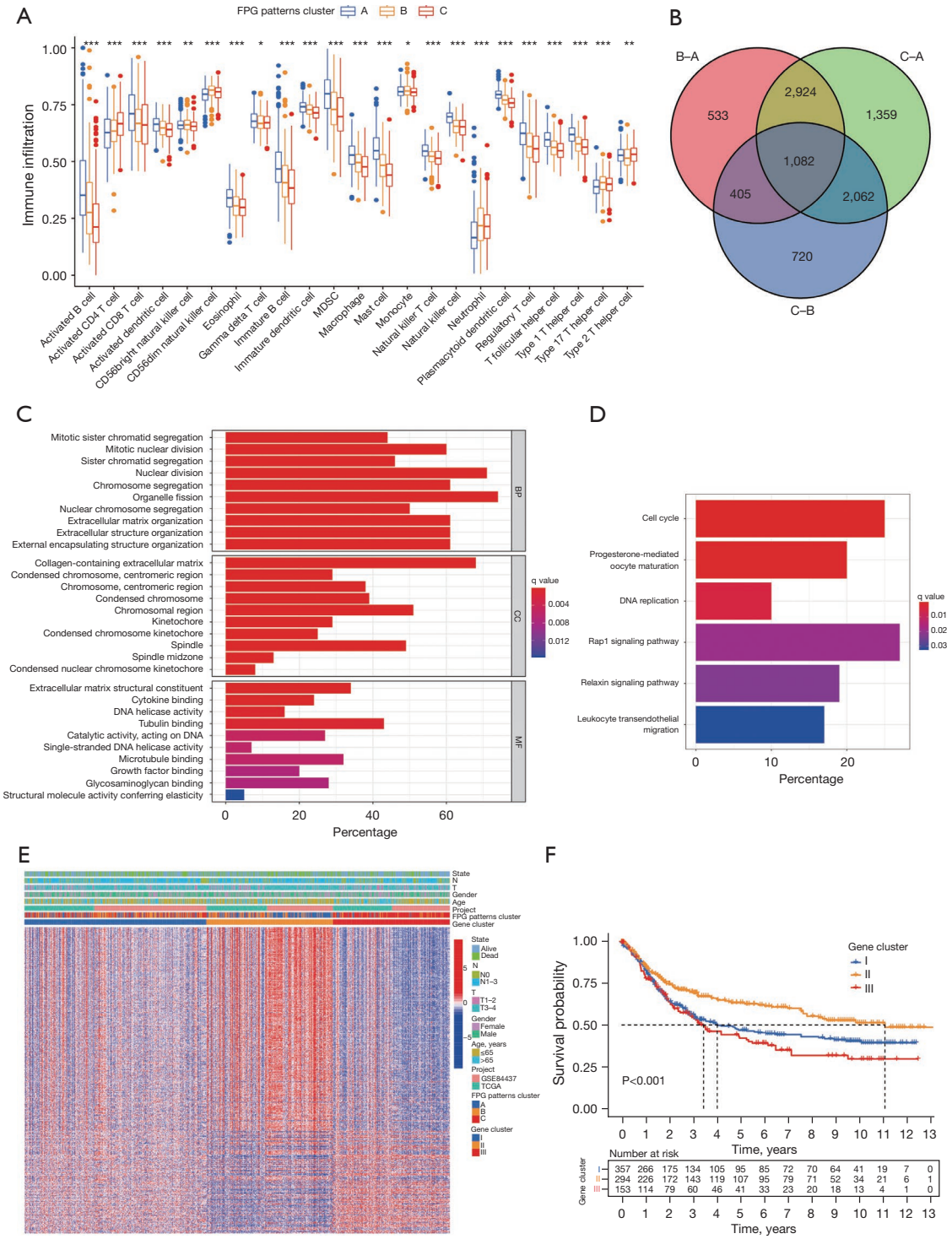

Figure 4 Characterization of TME cell infiltration and transcriptome features in three FPGs patterns. (A) The differential expression analysis of 23 immune cells among three FPGs patterns. ***, P<0.001; **, P<0.01; *, P<0.05. (B) Venn plots showing the overlapping genes in three FPGs patterns. (C) GO enrichment analysis of subtypes. (D) KEGG enrichment analysis of subtypes. (E) The heatmap of clinicopathologic characteristics and FPGs patterns. (F) Kaplan-Meier curves of the three gene clusters. MDSC, myeloid-derived suppressor cell; BP, biological process; CC, cellular component; MF, molecular function; FPG, ferroptosis and pyroptosis gene; TCGA, The Cancer Genome Atlas; TME, tumor microenvironment; GO, Gene Ontology; KEGG, Kyoto Encyclopedia of Genes and Genomes.

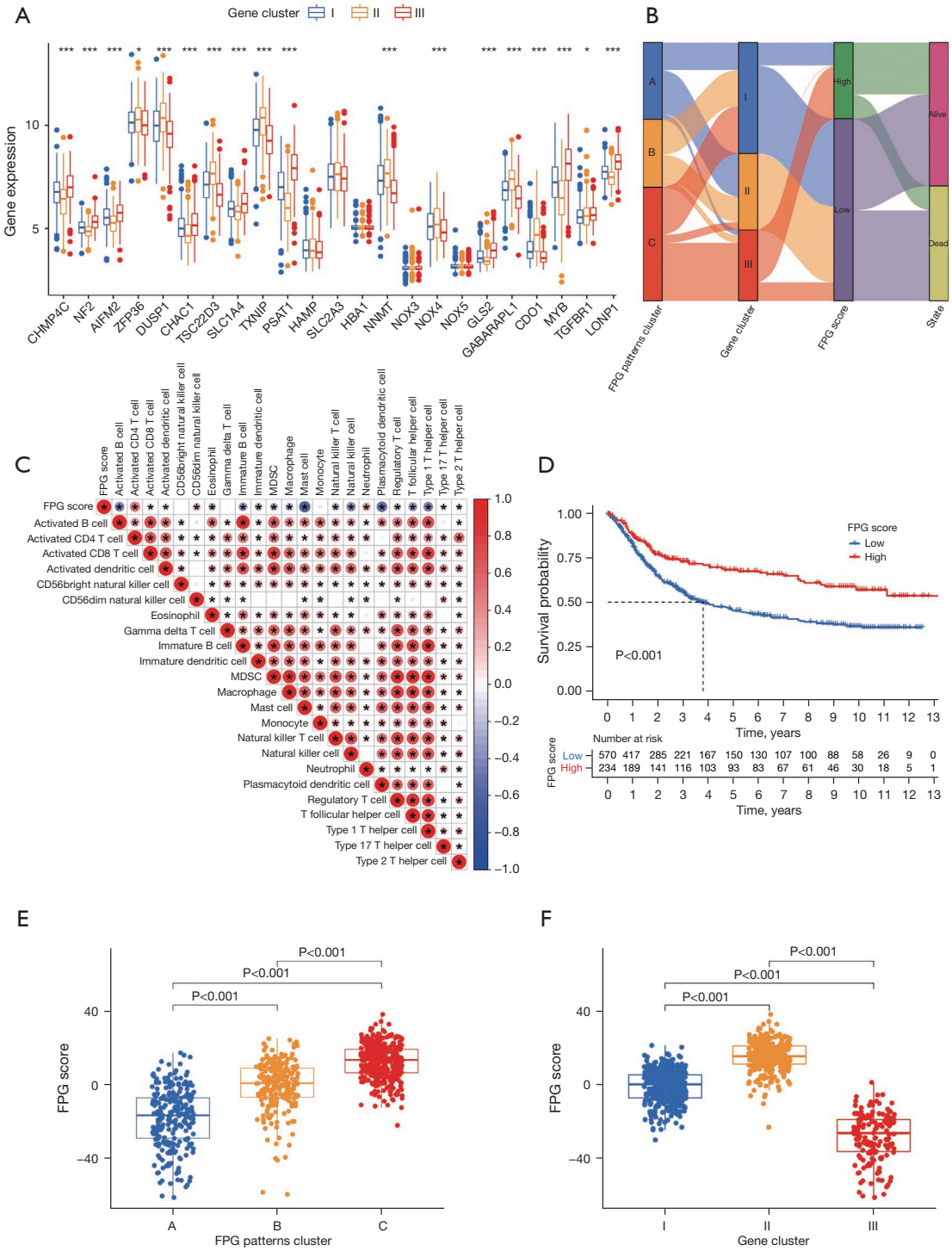

Figure 5 The development of ferroptosis and pyroptosis signature. (A) Differences in the expression of 23 FPGs among the three gene clusters. ***, P<0.001; *, P<0.05. (B) Sankey diagrams of different genotypes. (C) The correlation analysis between the FPG_Score and immune cells, * represents statistical significance; the larger the circle, the smaller the P value. (D) Survival analysis of the high FPG_Score group and low FPG_Score group. (E) Differential expression analysis of FPG_Score among the three FPGs patterns. (F) Differential expression analysis of FPG_Score among the three gene clusters. FPG, ferroptosis and pyroptosis gene; FPG_Score, ferroptosis/pyroptosis score; MDSC, myeloid-derived suppressor cell.

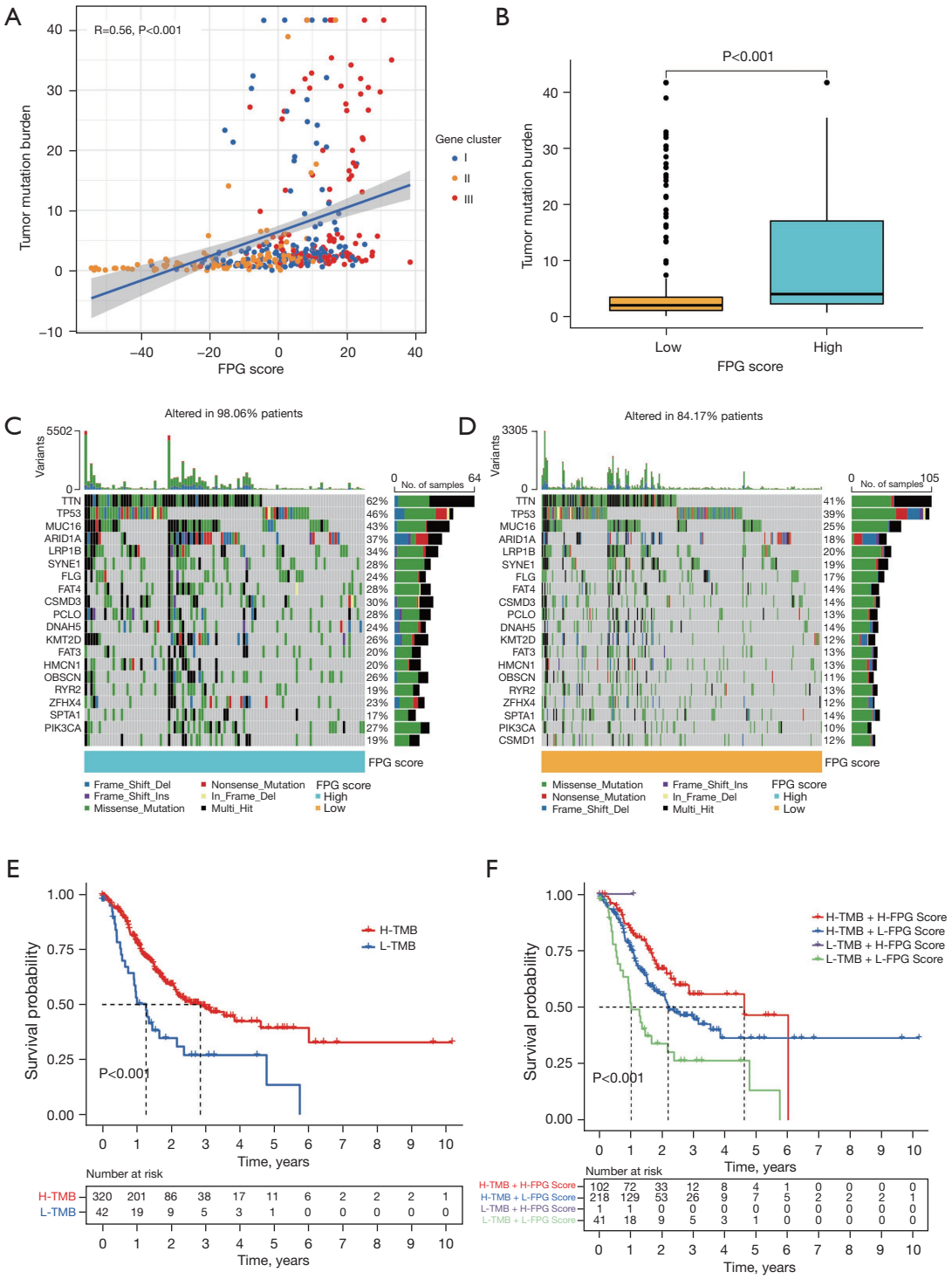

Figure 6 The characteristics of FPG_Score and TMB. (A) Spearman correlation analysis of the FPG_Score and TMB. (B) Correlations between FPG_Score and TMB calculated by CIBERSORT algorithm. (C,D) The waterfall plot displays the somatic mutation features that are stratified by high or low FPG_Score. The blue and yellow box represents high and low FPG_Score, respectively. The upper or right bar plot displayed the TMB and proportion of different mutation types, respectively. (E) Kaplan-Meier curves of survival probability of patients with gastric cancer in low or high TMB group. (F) Survival analysis among four groups of gastric cancer samples according to both levels of TMB combined with FPG_Score. FPG_Score, ferroptosis/pyroptosis score; H, high; L, low; TMB, tumor mutation burden.

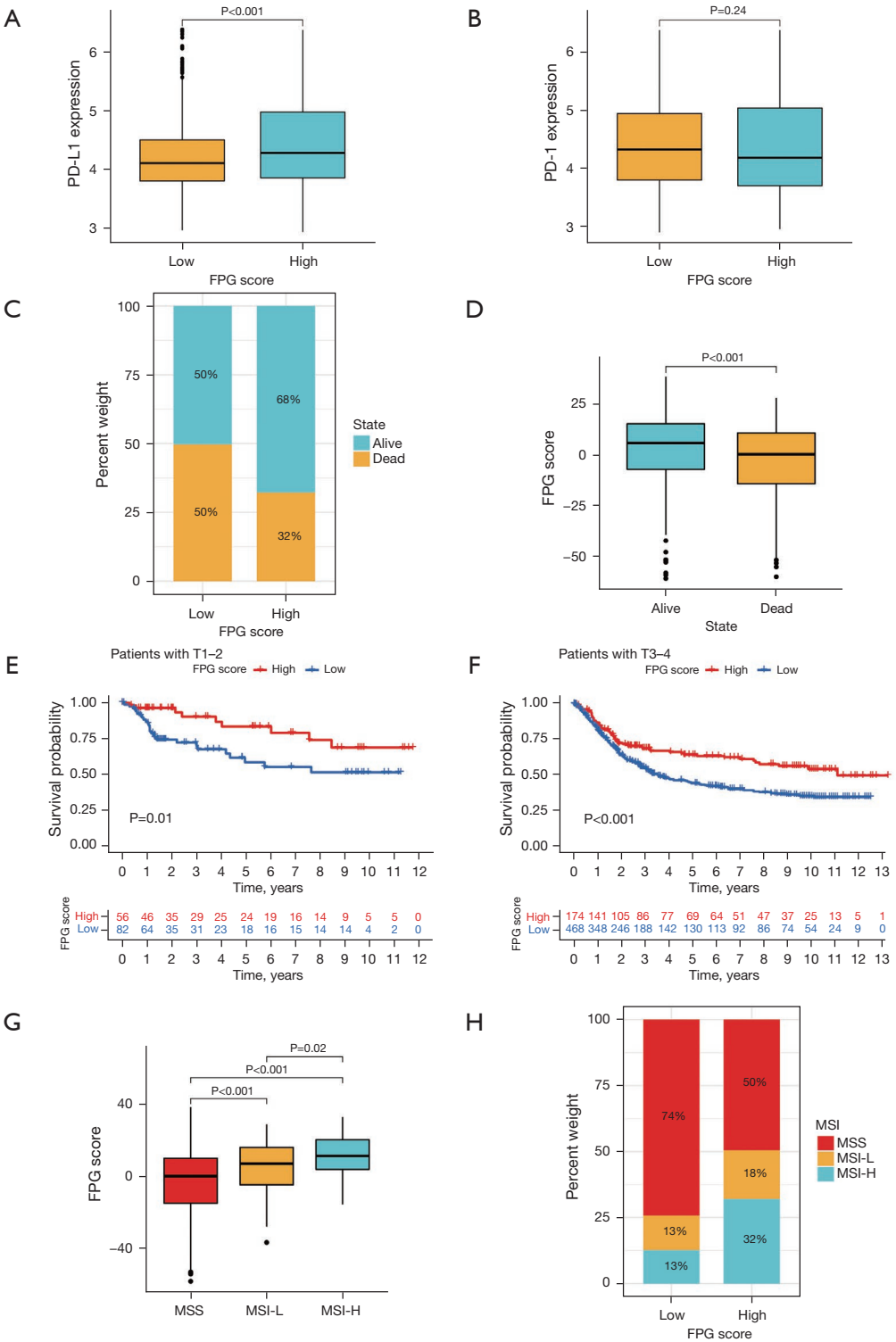

Figure 7 Comprehensive analysis of the prognostic value according to FPG_Score. (A,B) Expression levels of PD-L1 and PD-1 in the two FPG_Score groups. (C,D) Stratified analysis of the FPG_Score for GC patients by status. (E,F) Kaplan-Meier analysis of the FPG_Score for GC patients by T stages. (G,H) Relationships between FPG_Score, MSI, and MSS. FPG_Score, ferroptosis/pyroptosis score; PD-L1, programmed cell death protein ligand 1; PD-1, programmed cell death protein 1; MSS, microsatellite stability; MSI-L, low microsatellite instability; MSI-H, high microsatellite instability; GC, gastric cancer.

(*Figure 7E*,*7F*). Increasing evidence suggests that patients with high microsatellite instability (MSI-H), a biomarker for response to ICIs (34), are more sensitive to immunotherapy and get benefit from it. Correlation analysis revealed that a high FPG_Score was positively correlated with MSI-H status, while a low FPG_Score was associated with the status of microsatellite stable (MSS) (*Figure 7G*,*7H*), suggesting a benefit from immunotherapy for patients with high FPG_Score. Collectively, the FPGs may provide significant insights for tumor-targeted therapy with immunotherapy together.

Exploration of ferroptosis-pyroptosis related risk model in single-cell level

The protein-protein interaction (PPI) network was constructed by Cytoscape, and TXNIP, DUSP1 and ZFP36 were identified as core regulators in the established model (*Figure 8A*). Then, t-distributed stochastic neighbor embedding (t-SNE) was performed on principal components (PC0-13) to classify all cells into 14 clusters (*Figure 8B*). Epithelial cells, tissue stem cells, endothelial cell, hepatocytes, B cells, as well as smooth muscle cells were main cell types in these clusters (*Figure 8C*). The expression level of each ferroptosis-pyroptosis related gene in different clusters was displayed in *Figure 8D*. TXNIP highly expressed in endothelial cells, DUSP1 highly expressed in hepatocytes, and ZFP36 highly expressed in tissue stem cells (*Figure 8E*). The expression and percentage of ferroptosis-pyroptosis related genes in different cell subsets were showed in *Figure 8F*.

The combination of ferroptosis inducer and pyroptosis inducer can exert a synergistic anti-cancer effect

Emerging evidence shows that triggering ferroptosis and pyroptosis exert efficient antitumor activity (35,36). Our previous results showed that FPGs are vital for GC's prognosis. Hence, we treat BGC823 cells with erastin (ferroptosis inducer) and α-KG (pyroptosis inducer). The cell viability result indicated that erastin exhibits a synergistic effect with α-KG (*Figure 9A*,*9B*), presenting the promising value of combined therapies of ferroptosis and pyroptosis.

Discussion

Recently, increasing attentions have been focused on the ferroptosis and pyroptosis in the occurrence and progression of tumors. Yet the comprehensive effect and TME infiltration characteristics mediated by the combination of FPGs have not been fully understood. Therefore, this study aimed to study FPGs combined with TME in GC patients, which will guide more effective tumor-targeted immunotherapy strategies and prognosis evaluation. Firstly, we analyzed the genetic and transcriptional alterations of the FPGs in GC. As previously reported, the expression abundance of FPGs, such as LONP1, GLS2, and METTL3 was higher in GC than in normal tissues (37-40). Similarly, LONP1 is revolved in ferroptosis via regulating GPX4 (38). Moreover, it has been reported that the expression of GLS2 inhibits ferroptosis and anti-tumorigenesis (39). METTL3 serves as a prognostic marker, which plays a significant role in the progression of GC (40). The high-risk genes include *NOX5*, *NOX3*, *NOX4*, and *HAMP*. NADPH oxidases (NOXs) are a family of transmembrane proteins that generate ROS (41). NOXs participate in numerous crucial physiological processes, including host defense, the post-translational processing of proteins, cellular signaling, regulation of gene expression, and cell differentiation (42). It is reported that patients with colon cancer had high NOX5 expression and poor prognosis (41). Hepcidin (HAMP), as a peptide hormone, plays a vital role in regulating systemic iron homeostasis (43). Recent new research suggests that high HAMP expression may serve as an independent prognostic biomarker through the immune pathway in patients with GC (43). These results indicated that FPGs might have the potential to act as a biomarker of GC.

According to the first consensus clustering, we recognized three FPGs patterns with prognostic differences based on the gene expression of FPGs. The survival analysis showed that FPGs pattern C had the best survival outcome, while FPGs pattern A had the worst. These results suggest that FPGs patterns were correlated with the prognosis of GC. Furthermore, immune analyses showed that the immune cell infiltration was significantly different among the three patterns. Li *et al.* (44) found that patients with well-differentiated GC had higher levels of CD4 T cells. Consistently, our results showed that the FPGs pattern A had higher activated B cells, activated CD8 T cells, activated DCs, γδT cells, immature B cells, immature DCs, and so on. These results reveal that the FPGs are involved in the shaping of the TME directly. Meanwhile, GO enrichment analysis and KEGG pathway analysis were performed according to the different genes of the three patterns, which showed that pattern-related DEGs were

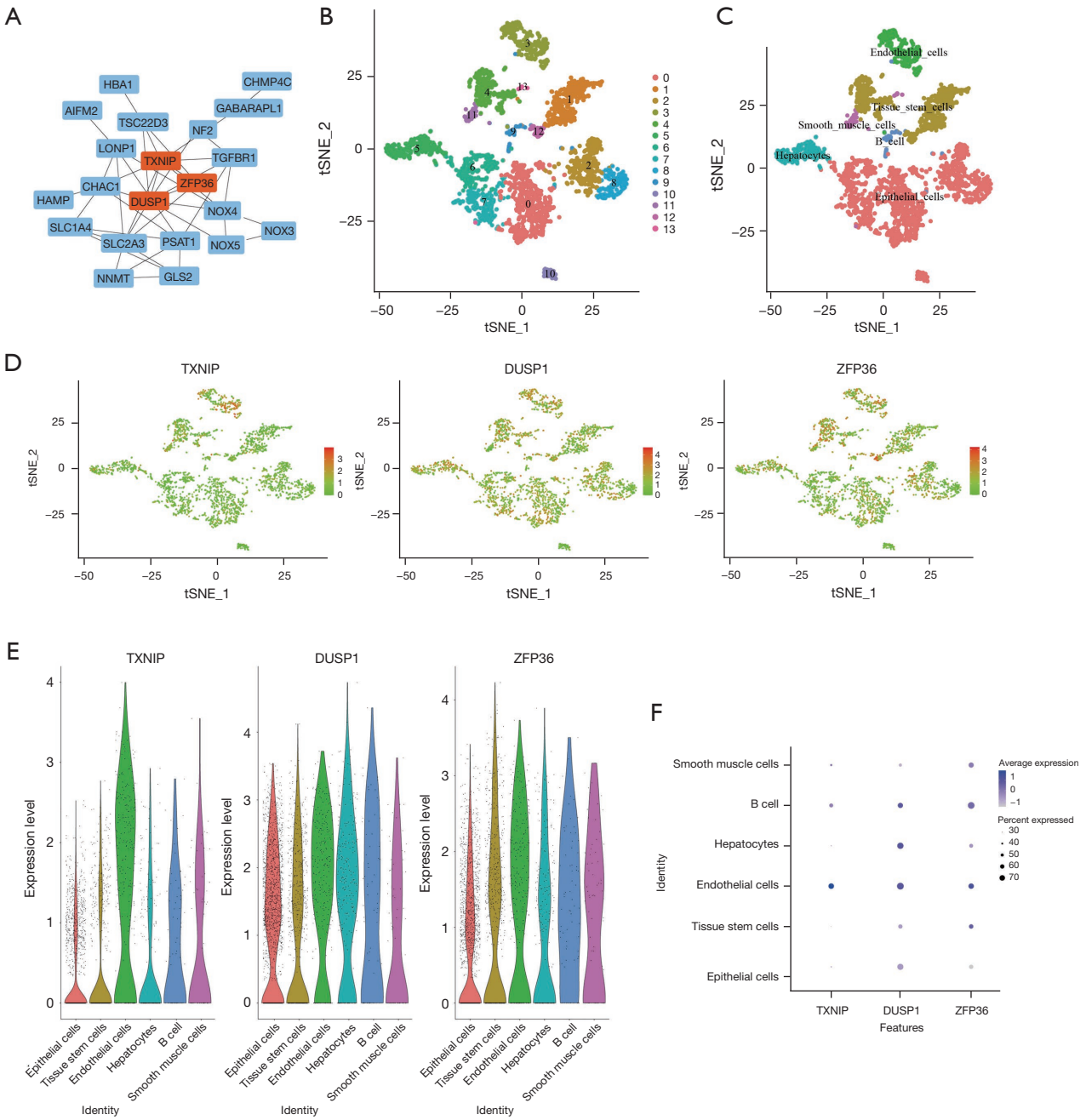

Figure 8 The expression of ferroptosis-pyroptosis-related genes in cell identities. (A) The PPI network for TXNIP and FPGs by Cytoscape. (B) Identification of cell clusters by t-SNE. (C) A cell annotation of clusters identified by t-SNE. (D) The expression level of each ferroptosis-pyroptosis-related risk model gene in different clusters. (E,F) The violin plot of expression of ferroptosis-pyroptosis-related genes in cell subsets 8F the bubble diagram of expression of ferroptosis-pyroptosis-related genes in cell subsets. t-SNE, t-distributed stochastic neighbor embedding; FPG, ferroptosis and pyroptosis gene; PPI, protein-protein interaction.

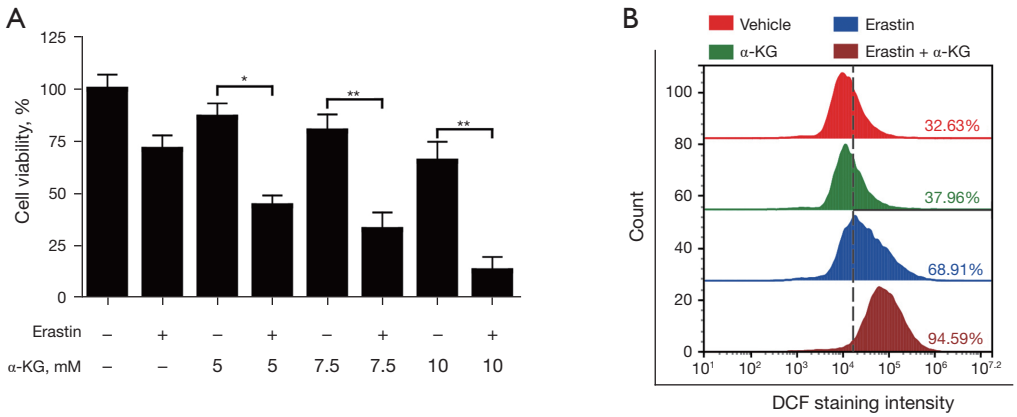

Figure 9 The combined effects of ferroptosis inducer and pyroptosis inducer on cell viability and ROS. (A) The BGC823 cells were exposed to erastin and α-KG, then cell viability was measured by CCK-8 assay. *, P<0.05; **, P<0.01. (B) The BGC823 cells were exposed to erastin and α-KG, and ROS level was measured by flow cytometry. α-KG, α-ketoglutarate; DCF, 2,7-dichlorofluorescein; ROS, reactive oxygen species; CCK-8, Cell Counting Kit-8.

involved in a variety of cellular and biological functions and affected the growth and proliferation of tumor cells. Moreover, via applying intersection analysis, three distinct gene subtypes based on DEGs were identified. The survival analysis showed that gene subtype II had the best survival outcome, while gene subtype III had the worst. Our results indicated that FPGs may be used as an indicator to predict the clinical outcome of GC. To assess the prognosis of GC patients steps further, we constructed a scoring model. Patients in low and high-risk FPG_Score group showed obviously different clinicopathological characteristics, prognosis, mutation, TME, immune checkpoints, MSS, and MSI index.

In recent years, more and more evidence has proved the important contribution of the TME to predicting cancer progression and therapeutic drug resistance (45), especially in GC (46). The regulation of inflammatory response caused by ferroptosis and pyroptosis plays an important role in the TME. ICIs have been applied as major treatment strategies for various malignant tumors. Currently, commonly used ICIs, including monoclonal antibodies inhibit PD-1, PD-L1, and CTLA-4 (47,48), and their safety and effectiveness have been proven by numerous clinical studies (49,50). Our results showed the expression level of PD-L1 in the high FPG_Score group was higher than that in the low FPG_Score group, indicating that patients in high FPG_Score are more likely to benefit from immune checkpoint therapies. TMB is defined as the number of somatic/acquired mutations per coding area of a tumor genome mutation per megabase (Mut/Mb) that were sequenced in specific cancer (51) and has emerged as a potential predictive biomarker of response to ICIs, especially in early-stage solid tumors. It's worth noting the evidence that TMB can be applied as a prognostic biomarker of GC (52). Interestingly, our results show that FPG_Score was positively correlated with TMB, which indicated patients in high FPG_Score group obtained better benefits from ICIs. The transcription factor p53 promotes pyroptosis to inhibit tumor growth in non-small cell lung cancer (NSCLC) patients (53,54). Ferroptosis is also induced by P53 in liver fibrosis and effectively inhibits hematopoietic stem cell (HSC) activation (55). These suggest that P53 is a key factor in the induction of pyroptosis and ferroptosis. Our study showed that the high FPG_Score has a higher mutation rate, indicating high mutation frequency genes including *TTN*, *TP53*, and *MUC16*, which can be used as targets for anti-tumor diagnosis.

MSI is caused by mismatched gene repeat sequences due to abnormal DNA mismatch repair mechanisms, which play an important role in tumorigenesis and progression (56). Moreover, MSI is considered to be closely related to the occurrence and development of a variety of tumors, including GC, colorectal cancer, endometrial cancer, and so on (52,57,58). What's more, MSI-H tumors were reported to show potential sensitivity to immunotherapy due to high TMB and high expression of immune checkpoints like PD-L1 (59). Previous study has shown that GC patients in the MSI-H group had unique clinicopathological features, were associated with the earlier stage, tended to be more sensitive to immune checkpoint therapies, and had better survival (60).

Our results showed that the MSI-H group had a higher FPG_Score, suggesting that patients in the high FPG_Score group are more likely to benefit from immune checkpoint therapies. We also observed that the high FPG_Score group had higher levels of PD-L1 expression and were more susceptible to immune checkpoint therapy including PD-L1 and CTLA-4 immunotherapy. Above all, the high FPG_Score group had a longer survival time, higher TMB, higher expression of PD-L1, and a larger proportion of MSI-H. These results suggest that FPG_Score may be an independent and effective prognostic biomarker for GC, and FPGs may be used as diagnostic markers to provide new directions for tumor-targeted immunotherapy for GC. Despite a comprehensive evaluation and analysis using multiple platforms and databases, there are limitations and the conclusions need further experiments to elucidate the underlying mechanisms.

Conclusions

Inducing programmed death of tumor cells is an important way of anti-cancer therapy. We innovatively combined ferroptosis and pyroptosis and constructed a scoring system to predict the prognosis and response to immunotherapy. This study provides some new insights to formulate immunotherapy interventions for GC patients.

Acknowledgments

Funding: This research was supported by the Medical and Health Science and Technology Project of Zhejiang Province (Nos. 2024XY184, 2024KY725); Health Science and Technology project of Shaoxing City (No. 2023SKY121); and Medical and Health research project of Zhuji City (No. 2023YW118).

Footnote

Reporting Checklist: The authors have completed the TRIPOD reporting checklist. Available at https://tcr.amegroups.com/article/view/10.21037/tcr-24-683/rc

Peer Review File: Available at https://tcr.amegroups.com/article/view/10.21037/tcr-24-683/prf

Conflicts of Interest: All authors have completed the ICMJE uniform disclosure form (available at https://tcr.amegroups.com/article/view/10.21037/tcr-24-683/coif). G.W. is a member of the Adicon Clinical Laboratories, Inc. The other authors have no conflicts of interest to declare.

Ethical Statement: The authors are accountable for all aspects of the work in ensuring that questions related to the accuracy or integrity of any part of the work are appropriately investigated and resolved. The study was conducted in accordance with the Declaration of Helsinki (as revised in 2013).

References

1. Joshi SS, Badgwell BD. Current treatment and recent progress in gastric cancer. CA Cancer J Clin 2021;71:264-79.
2. Zeng R, Gou H, Lau HCH, et al. Stomach microbiota in gastric cancer development and clinical implications. Gut 2024;gutjnl-2024-332815.
3. Wu H, Fu M, Liu J, et al. The role and application of small extracellular vesicles in gastric cancer. Mol Cancer 2021;20:71.
4. Hu W, Zhou C, Jing Q, et al. FTH promotes the proliferation and renders the HCC cells specifically resist to ferroptosis by maintaining iron homeostasis. Cancer Cell Int 2021;21:709.
5. Li Y, Wang X, Huang Z, et al. CISD3 inhibition drives cystine-deprivation induced ferroptosis. Cell Death Dis 2021;12:839.
6. Du J, Wang X, Li Y, et al. DHA exhibits synergistic therapeutic efficacy with cisplatin to induce ferroptosis in pancreatic ductal adenocarcinoma via modulation of iron metabolism. Cell Death Dis 2021;12:705.
7. Du J, Zhou Y, Li Y, et al. Identification of Frataxin as a regulator of ferroptosis. Redox Biol 2020;32:101483.
8. Du J, Wang T, Li Y, et al. DHA inhibits proliferation and induces ferroptosis of leukemia cells through autophagy dependent degradation of ferritin. Free Radic Biol Med 2019;131:356-69.
9. Ren X, Li Y, Zhou Y, et al. Overcoming the compensatory

elevation of NRF2 renders hepatocellular carcinoma cells more vulnerable to disulfiram/copper-induced ferroptosis. Redox Biol 2021;46:102122.
10. Li Y, Xia J, Shao F, et al. Sorafenib induces mitochondrial dysfunction and exhibits synergistic effect with cysteine depletion by promoting HCC cells ferroptosis. Biochem Biophys Res Commun 2021;534:877-84.
11. Xia X, Fan X, Zhao M, et al. The Relationship between Ferroptosis and Tumors: A Novel Landscape for Therapeutic Approach. Curr Gene Ther 2019;19:117-24.
12. Cookson BT, Brennan MA. Pro-inflammatory programmed cell death. Trends Microbiol 2001;9:113-4.
13. Rogers C, Fernandes-Alnemri T, Mayes L, et al. Cleavage of DFNA5 by caspase-3 during apoptosis mediates progression to secondary necrotic/pyroptotic cell death. Nat Commun 2017;8:14128.
14. Erkes DA, Cai W, Sanchez IM, et al. Mutant BRAF and MEK Inhibitors Regulate the Tumor Immune Microenvironment via Pyroptosis. Cancer Discov 2020;10:254-69.
15. Wang Q, Wang Y, Ding J, et al. A bioorthogonal system reveals antitumour immune function of pyroptosis. Nature 2020;579:421-6.
16. Tang R, Xu J, Zhang B, et al. Ferroptosis, necroptosis, and pyroptosis in anticancer immunity. J Hematol Oncol 2020;13:110.
17. Deng BB, Jiao BP, Liu YJ, et al. BIX-01294 enhanced chemotherapy effect in gastric cancer by inducing GSDME-mediated pyroptosis. Cell Biol Int 2020;44:1890-9.
18. Lang X, Green MD, Wang W, et al. Radiotherapy and Immunotherapy Promote Tumoral Lipid Oxidation and Ferroptosis via Synergistic Repression of SLC7A11. Cancer Discov 2019;9:1673-85.
19. Zhou Z, He H, Wang K, et al. Granzyme A from cytotoxic lymphocytes cleaves GSDMB to trigger pyroptosis in target cells. Science 2020;368:eaaz7548.
20. Liao P, Wang W, Wang W, et al. CD8(+) T cells and fatty acids orchestrate tumor ferroptosis and immunity via ACSL4. Cancer Cell 2022;40:365-378.e6.
21. Gao W, Wang X, Zhou Y, et al. Autophagy, ferroptosis, pyroptosis, and necroptosis in tumor immunotherapy. Signal Transduct Target Ther 2022;7:196.
22. Jiang C, Zhang N, Hu X, et al. Tumor-associated exosomes promote lung cancer metastasis through multiple mechanisms. Mol Cancer 2021;20:117.
23. Liu LP, Lu L, Zhao QQ, et al. Identification and Validation of the Pyroptosis-Related Molecular Subtypes of Lung Adenocarcinoma by Bioinformatics and Machine Learning. Front Cell Dev Biol 2021;9:756340.
24. Zhou C, Wang L, Hu W, et al. CDC25C is a prognostic biomarker and correlated with mitochondrial homeostasis in pancreatic adenocarcinoma. Bioengineered 2022;13:13089-107.
25. Ye Y, Dai Q, Qi H. A novel defined pyroptosis-related gene signature for predicting the prognosis of ovarian cancer. Cell Death Discov 2021;7:71.
26. Hu J, Lai C, Shen Z, et al. A Prognostic Model of Bladder Cancer Based on Metabolism-Related Long Non-Coding RNAs. Front Oncol 2022;12:833763.
27. Liberzon A, Birger C, Thorvaldsdóttir H, et al. The Molecular Signatures Database (MSigDB) hallmark gene set collection. Cell Syst 2015;1:417-25.
28. Rooney MS, Shukla SA, Wu CJ, et al. Molecular and genetic properties of tumors associated with local immune cytolytic activity. Cell 2015;160:48-61.
29. Yang J, Dai X, Xu H, et al. Regulation of Ferroptosis by Amino Acid Metabolism in Cancer. Int J Biol Sci 2022;18:1695-705.
30. Bagchi S, Yuan R, Engleman EG. Immune Checkpoint Inhibitors for the Treatment of Cancer: Clinical Impact and Mechanisms of Response and Resistance. Annu Rev Pathol 2021;16:223-49.
31. Merino DM, McShane LM, Fabrizio D, et al. Establishing guidelines to harmonize tumor mutational burden (TMB): in silico assessment of variation in TMB quantification across diagnostic platforms: phase I of the Friends of Cancer Research TMB Harmonization Project. J Immunother Cancer 2020;8:e000147.
32. Allgäuer M, Budczies J, Christopoulos P, et al. Implementing tumor mutational burden (TMB) analysis in routine diagnostics-a primer for molecular pathologists and clinicians. Transl Lung Cancer Res 2018;7:703-15.
33. Wang X, Wu WKK, Gao J, et al. Autophagy inhibition enhances PD-L1 expression in gastric cancer. J Exp Clin Cancer Res 2019;38:140.
34. Schrock AB, Ouyang C, Sandhu J, et al. Tumor mutational burden is predictive of response to immune checkpoint inhibitors in MSI-high metastatic colorectal cancer. Ann Oncol 2019;30:1096-103.
35. Liang C, Zhang X, Yang M, et al. Recent Progress in Ferroptosis Inducers for Cancer Therapy. Adv Mater 2019;31:e1904197.
36. Li L, Jiang M, Qi L, et al. Pyroptosis, a new bridge to tumor immunity. Cancer Sci 2021;112:3979-94.
37. Hao S, Yu J, He W, et al. Cysteine Dioxygenase 1

Mediates Erastin-Induced Ferroptosis in Human Gastric Cancer Cells. Neoplasia 2017;19:1022-32.
38. Yao F, Zhan Y, Pu Z, et al. LncRNAs Target Ferroptosis-Related Genes and Impair Activation of CD4(+) T Cell in Gastric Cancer. Front Cell Dev Biol 2021;9:797339.
39. Niu Y, Zhang J, Tong Y, Li J, Liu B. Physcion 8-O-β-glucopyranoside induced ferroptosis via regulating miR-103a-3p/GLS2 axis in gastric cancer. Life sciences. 2019 Nov 15;237:116893. PubMed PMID: 31606381. Epub 2019/10/14. eng.
40. Liu T, Yang S, Sui J, et al. Dysregulated N6-methyladenosine methylation writer METTL3 contributes to the proliferation and migration of gastric cancer. J Cell Physiol 2020;235:548-62.
41. Ashizawa N, Shimizu H, Shoda K, et al. NADPH oxidase 5 has a crucial role in cellular motility of colon cancer cells. Int J Oncol 2021;59:63.
42. Vermot A, Petit-Härtlein I, Smith SME, et al. NADPH Oxidases (NOX): An Overview from Discovery, Molecular Mechanisms to Physiology and Pathology. Antioxidants (Basel) 2021;10:890.
43. Pi M, Kuang H, Yue C, et al. Targeting metabolism to overcome cancer drug resistance: A promising therapeutic strategy for diffuse large B cell lymphoma. Drug Resist Updat 2022;61:100822.
44. Li F, Sun Y, Huang J, et al. CD4/CD8 + T cells, DC subsets, Foxp3, and IDO expression are predictive indictors of gastric cancer prognosis. Cancer Med 2019;8:7330-44.
45. Runa F, Hamalian S, Meade K, et al. Tumor microenvironment heterogeneity: challenges and opportunities. Curr Mol Biol Rep 2017;3:218-29.
46. Morihiro T, Kuroda S, Kanaya N, et al. PD-L1 expression combined with microsatellite instability/CD8+ tumor infiltrating lymphocytes as a useful prognostic biomarker in gastric cancer. Sci Rep 2019;9:4633.
47. Rotte A. Combination of CTLA-4 and PD-1 blockers for treatment of cancer. J Exp Clin Cancer Res 2019;38:255.
48. Yaghoubi N, Soltani A, Ghazvini K, et al. PD-1/ PD-L1 blockade as a novel treatment for colorectal cancer. Biomed Pharmacother 2019;110:312-8.
49. Yuan C, Yuan M, Chen M, et al. Prognostic Implication of a Novel Metabolism-Related Gene Signature in Hepatocellular Carcinoma. Front Oncol 2021;11:666199.
50. Zhang S, Zheng W, Jiang D, et al. Systematic Chromatin Accessibility Analysis Based on Different Immunological Subtypes of Clear Cell Renal Cell Carcinoma. Front Oncol 2021;11:575425.
51. Addeo A, Friedlaender A, Banna GL, et al. TMB or not TMB as a biomarker: That is the question. Crit Rev Oncol Hematol 2021;163:103374.
52. Puliga E, Corso S, Pietrantonio F, et al. Microsatellite instability in Gastric Cancer: Between lights and shadows. Cancer Treat Rev 2021;95:102175.
53. Zhang T, Li Y, Zhu R, et al. Transcription Factor p53 Suppresses Tumor Growth by Prompting Pyroptosis in Non-Small-Cell Lung Cancer. Oxid Med Cell Longev 2019;2019:8746895.
54. Wellenstein MD, Coffelt SB, Duits DEM, et al. Loss of p53 triggers WNT-dependent systemic inflammation to drive breast cancer metastasis. Nature 2019;572:538-42.
55. Wang L, Zhang Z, Li M, et al. P53-dependent induction of ferroptosis is required for artemether to alleviate carbon tetrachloride-induced liver fibrosis and hepatic stellate cell activation. IUBMB Life 2019;71:45-56.
56. Kok M, Chalabi M, Haanen J. How I treat MSI cancers with advanced disease. ESMO Open 2019;4:e000511.
57. Cohen R, Rousseau B, Vidal J, et al. Immune Checkpoint Inhibition in Colorectal Cancer: Microsatellite Instability and Beyond. Target Oncol 2020;15:11-24.
58. Kahn RM, Gordhandas S, Maddy BP, et al. Universal endometrial cancer tumor typing: How much has immunohistochemistry, microsatellite instability, and MLH1 methylation improved the diagnosis of Lynch syndrome across the population? Cancer 2019;125:3172-83.
59. Rodriquenz MG, Roviello G, D'Angelo A, et al. MSI and EBV Positive Gastric Cancer's Subgroups and Their Link With Novel Immunotherapy. J Clin Med 2020;9:1427.
60. Chen TH, Chen MH, Hung YP, et al. Elevated PD-L1 Expression and Microsatellite Instability in Elderly Patients With Gastric Cancer. J Immunother 2023;46:111-9.

Cite this article as: Shi H, Yao H, Zhou Y, Wu G, Li K, Tang L, Yang C, Wang D, Jin W. Construction of ferroptosis and pyroptosis model to assess the prognosis of gastric cancer patients based on bioinformatics. Transl Cancer Res 2024;13(11):5751-5770. doi: 10.21037/tcr-24-683

